PHYSICAL REVIEW D **89,** 126006 (2014)

Enhancement of jet quenching around phase transition: Result from the dynamical holographic model

Danning Li,[1] Jinfeng Liao,[2,3] and Mei Huang[1,4]

[1]*Institute of High Energy Physics, Chinese Academy of Sciences, 100049 Beijing, People's Republic of China*

[2]*Physics Department, Center for Exploration of Energy and Matter, Indiana University, 2401 North Milo B. Sampson Lane, Bloomington, Indiana 47408, USA*

[3]*RIKEN BNL Research Center, Building 510 A, Brookhaven National Laboratory, Upton, New York 11973, USA*

[4]*Theoretical Physics Center for Science Facilities, Chinese Academy of Sciences, 100049 Beijing, People's Republic of China*

(Received 15 January 2014; published 25 June 2014)

The phase transition and jet quenching parameter $\hat{q}$ are investigated in the framework of the dynamical holographic QCD model. We find that both the trace anomaly and the ratio of the jet quenching parameter over cubic temperature $\hat{q}/T^3$ show a peak around the critical temperature T_c, and the ratio of the jet quenching parameter over entropy density $\hat{q}/s$ sharply rises at T_c. This indicates that the jet quenching parameter can characterize the phase transition. The effect of the jet quenching parameter enhancement around the phase transition on the nuclear modification factor R_{AA} and elliptic flow v_2 are also analyzed, and we find that the temperature-dependent jet quenching parameter from the dynamical holographic QCD model can considerably improve the description of jet quenching azimuthal anisotropy as compared with the conformal case.

DOI: 10.1103/PhysRevD.89.126006 PACS numbers: 11.25.Tq, 12.38.Lg, 12.38.Mh

I. INTRODUCTION

Studying the quantum chromodynamics (QCD) phase transition and properties of hot/dense quark matter at high temperature has been the main target of heavy ion collision experiments at the Relativistic Heavy Ion Collider (RHIC) and the Large Hadron Collider (LHC). It is now believed that the system created at the RHIC and LHC is a strongly coupled quark-gluon plasma (sQGP) and behaves like a nearly "perfect" fluid [1,2].

The collective flow v_2 of the highly excited and strongly interacting matter formed at the RHIC can be well described by relativistic hydrodynamics with a negligible ratio of shear viscosity over entropy density η/s [3]. A lattice QCD calculation confirmed that η/s for the purely gluonic plasma is rather small and in the range of 0.1–0.2 [4]. Shear viscosity η characterizes how strongly particles interact and move collectively in a many-body system. In general, the stronger the interparticle interaction, the smaller the ratio of shear viscosity over entropy density. Another unusual feature of the strongly interacting matter formed at the RHIC is that the emission of hadrons with large transverse momentum is strongly suppressed in central collisions [5]. The suppression of hadrons at large transverse momentum is normally referred to as jet quenching, which characterizes the squared average transverse momentum exchange between the medium and the fast parton per unit path length [6]. The current knowledge on jet quenching is that it is caused by gluon radiation induced by multiple collisions of the leading parton with color charges in the near-thermal medium [6–8]. Therefore, jet quenching can tell us the properties of the created hot dense matter by the energetic parton passing through the medium.

It is very interesting to ask whether transport quantities can characterize phase transitions. It has been observed that the shear-viscosity-over-entropy-density ratio η/s has a minimum in the phase transition region in systems of water, helium, nitrogen [9], and many other substances [10]. It has been shown that η/s is suppressed near the critical temperature in the semi-quark-gluon plasma [11], and η/s can characterize first- and second-order phase transitions and crossover [12], i.e.,η/s shows a cusp, a jump at T_c, and a shallow valley around T_c, respectively.

In Ref. [13], it has been suggested that the jet quenching parameter can also be used to measure the coupling strength of the medium and a general relation between the shear viscosity η/s and the jet quenching parameter $\hat{q}/T^3$ for a quasiparticle-dominated quark-gluon plasma the relation has been derived, i.e.,$\eta/s \sim T^3/\hat{q}$. The relation associates a small ratio of shear viscosity to entropy density to a large value of the jet quenching parameter. If we naively extend this relation to the critical temperature region, we expect that $\hat{q}/T^3$ will show a peak around the critical temperature T_c. Furthermore, the validity of this extension can be seen from anisotropic holographic studies [14,15], where similar behavior of the violation of the lower bound of the ratio η/s and the violation of the universal properties of the Langevin diffusion coefficients, in some sense, indicates the close relation of these variables in a

strongly coupled region. Phenomenologically, the strong near-T_c-enhancement (NTcE) scenario of jet-medium interaction [16] was proposed in the efforts to explain the large jet quenching anisotropy at high p_t at the RHIC [17–20]. More recently, it was shown in Refs. [21,22] that the NTcE model naturally induces a reduction (∼30%) of jet-medium interaction strength from the RHIC to LHC.

It is worth mentioning that another transport coefficient, the bulk viscosity ζ/s, also exhibits a sharp rising behavior around the critical temperature T_c as shown in lattice QCD [23–25], the linear sigma model [26], the Polyakov-loop linear sigma model [27], and the real scalar model [28]. The rising of bulk viscosity near the phase transition corresponds to the peak of the trace anomaly around T_c, which shows the equation of state is highly nonconformal [29,30] around the phase transition.

Because of the complexity of QCD in the regime of strong coupling, in recent years, the anti–de Sitter/conformal field theory (AdS/CFT) correspondence [31–33] has generated enormous interest in using thermal $\mathcal{N}=4$ super-Yang-Mills theory (SYM) to understand sQGP. However, a conspicuous shortcoming of this approach is the conformality of SYM: the square of the speed of sound c_s^2 always equals $1/3$, the bulk viscosity is always zero at all temperatures in this theory, and $\eta/s=\frac{1}{4\pi}$ [34] and $\hat{q}/T^3 \simeq 7.53\sqrt{\lambda}$ ($\lambda = g_{YM}^2 N_c$ the 't Hooft coupling) [35] remains constant for all temperatures. In order to describe the nonconformal properties near the phase transition and mimic the QCD equation of state, much effort has been made to find the gravity dual of gauge theories which break the conformal symmetry, e.g., Refs. [36–39], where a real scalar dilaton field background has been introduced to couple with the graviton. References [36, 37] have used different dilaton potentials as input, Ref. [38] has used a QCD β function as input, and Ref. [39] has introduced a deformed metric background.

On the other hand, much effort has also been made to establish a more realistic holographic QCD model for glueball spectra and meson spectra [40–44]. Recently, a dynamical holographic QCD model [45–47] has been developed by mimicking the evolution of the renormalization group from ultraviolet (UV) regime to infrared regime (IR). The dynamical holographic QCD model is constructed in the graviton-dilaton-scalar framework, where the dilaton background field Φ and scalar field X are responsible for the gluodynamics and chiral dynamics, respectively. At the UV boundary, the dilaton field is dual to the dimension-four gluon operator, and the scalar field is dual to the dimension-three quark-antiquark operator. The metric structure at IR regime is automatically deformed by the nonperturbative gluon condensation and chiral condensation in the vacuum. The produced scalar glueball spectra in the graviton-dilaton framework agree well with the lattice data, and the light-flavor meson spectra generated in the graviton-dilaton-scalar framework are in good agreement with the experimental data. Both the chiral symmetry breaking and linear confinement are realized in this dynamical holographic QCD model.

In this work, we will investigate the phase transition, equation of state, and calculate the jet quenching parameter in the dynamical holographic QCD model. The paper is organized as follows. In Sec. II, we briefly introduce the dynamical holographic QCD model for a pure gluon system and a light-flavor system. In Sec. III, we will investigate the phase transition and equation of state, including the entropy density, the pressure density, and the energy density for the pure gluon system. Then, in Secs. IV–VI, we calculate jet quenching parameter and investigate the nuclear modification factor R_{AA} and elliptic flow v_2. The summary and discussion are given in Sec. VII.

II. DYNAMICAL HOLOGRAPHIC QCD MODEL

QCD in terms of quark and gluon degrees of freedom is accepted as the fundamental theory of the strong interaction. In the UV or weak coupling regime of QCD, the perturbative calculations for deep inelastic scattering agree well with the experimental data. However, in the IR regime, the description of the QCD vacuum as well as hadron properties and nonperturbative processes still remains an outstanding challenge in the formulation of QCD as a local quantum field theory. In the past half century, various nonperturbative methods have been developed, in particular, lattice QCD, Dyson-Schwinger equations, and functional renormalization group equations. In recent decades, an entirely new method based on the AdS/CFT correspondence and the conjecture of the gravity/gauge duality [31–33] provides a revolutionary method to tackle the problem of strongly coupled gauge theories.

In general, holography relates quantum field theory (QFT) in d dimensions to quantum gravity in $(d+1)$ dimensions, with the gravitational description becoming classical when the QFT is strongly coupled. The extra dimension can be interpreted as an energy scale or renormalization group (RG) flow in the QFT [48].

The recently developed dynamical holographic QCD model [45,46] can resemble the renormalization group from UV to IR, as shown in Fig. 1 [47]. The dilaton background $\Phi(z)$ is introduced to describe the gluodynamics, and the scalar field $X(z)$ is responsible for chiral dynamics, respectively.

For the pure gluon system, we construct the quenched dynamical holographic QCD model in the graviton-dilaton framework by introducing one scalar dilaton field $\Phi(z)$ in the bulk. The 5D graviton-dilaton coupled action in the string frame is given below:

$$S_G = \frac{1}{16\pi G_5}\int d^5x\sqrt{g_s}e^{-2\Phi}(R_s + 4\partial_M\Phi\partial^M\Phi - V_G^s(\Phi)), \tag{1}$$

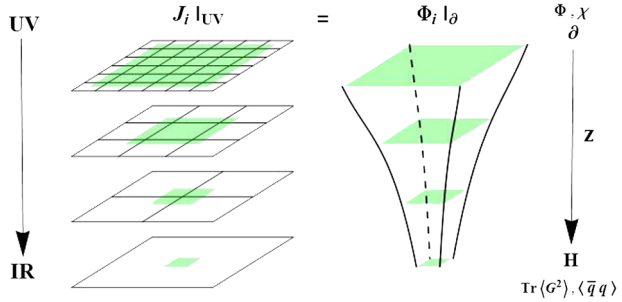

FIG. 1 (color online). Duality between d-dimension QFT and $(d+1)$-dimension gravity as shown in Ref. [48] (left-hand side). Dynamical holographic QCD model resembles the RG from UV to IR (right-hand side): At the UV boundary, the dilaton bulk field $\Phi(z)$ and scalar field $X(z)$ are dual to the dimension-four gluon operator and dimension-three quark-antiquark operator, which develop condensates at IR regime.

where G_5 is the 5D Newton constant, and g_s, Φ, and V_G^s are the 5D metric, the dilaton field, and the dilaton potential in the string frame, respectively. The metric ansatz is often chosen to be

$$ds^2 = e^{2A_s(z)}(dz^2 + \eta_{\mu\nu}dx^\mu dx^\nu). \tag{2}$$

In this paper, the capital letters like "M and N" stand for all the coordinates (0,1,..,4), and the greek indices stand for the 4D coordinates (0,…,3). We use the convention $\eta^{00} = \eta_{00} = -1$, $\eta^{ij} = \eta_{ij} = \delta_{ij}$.

To avoid the gauge noninvariant problem and to meet the requirement of gauge/gravity duality, we take the dilaton field in the form of

$$\Phi(z) = \mu_G^2 z^2 \tanh(\mu_{G^2}^4 z^2/\mu_G^2). \tag{3}$$

In this way, the dilaton field at UV regime behaves $\Phi(z) \overset{z\to 0}{\to} \mu_{G^2}^4 z^4$ and is dual to the dimension-four gauge invariant gluon operator $\mathrm{Tr}G^2$, while at IR regime it takes the quadratic form $\Phi(z) \overset{z\to\infty}{\to} \mu_G^2 z^2$. The equations of motion can be derived as

$$-A_s'' - \frac{4}{3}\Phi' A_s' + A_s^2 + \frac{2}{3}\Phi'' = 0, \tag{4}$$

$$\Phi'' + (3A_s' - 2\Phi')\Phi' - \frac{3}{8}e^{2A_s - \frac{4}{3}\Phi}\partial_\Phi(e^{\frac{4}{3}\Phi}V_G^s(\Phi)) = 0. \tag{5}$$

By self-consistently solving the Einstein equations, the metric structure A_s will be automatically deformed at IR regime by the dilaton background field or the nonperturbative gluodynamics. It is found in Ref. [46] that the scalar glueball spectra in the quenched dynamical model are in very good agreement with the lattice data. For details, please refer to Ref. [46].

To describe the two-flavor system, we then add light flavors in terms of the meson fields on the gluodynamical background. The total 5D action for the graviton-dilaton-scalar system takes the following form:

$$S = S_G + \frac{N_f}{N_c}S_{KKSS}. \tag{6}$$

Here, S_G is the 5D action for gluons in terms of the dilaton field Φ and takes the same form as Eq. (1), and S_{KKSS} is the 5D action for mesons propagating on the dilaton background and takes the same form as in the Karch-Katz-Son-Stephanov (KKSS) model [41]

$$S_{KKSS} = -\int d^5x\sqrt{g_s}e^{-\Phi}\mathrm{Tr}\left(|DX|^2 + V_X(X^+X,\Phi) + \frac{1}{4g_5^2}(F_L^2 + F_R^2)\right). \tag{7}$$

The difference here is that the metric structure A_s is solved from the following coupled equations of motion:

$$-A_s'' + A_s'^2 + \frac{2}{3}\Phi'' - \frac{4}{3}A_s'\Phi' - \frac{\lambda_0}{6}e^\Phi\chi'^2 = 0, \tag{8}$$

$$\Phi'' + (3A_s' - 2\Phi')\Phi' - \frac{3\lambda_0}{16}e^\Phi\chi'^2 - \frac{3}{8}e^{2A_s - \frac{4}{3}\Phi}\partial_\Phi(V_G(\Phi) + \lambda_0 e^{\frac{7}{3}\Phi}V_C(\chi,\Phi)) = 0, \tag{9}$$

$$\chi'' + (3A_s' - \Phi')\chi' - e^{2A_s}V_{C,\chi}(\chi,\Phi) = 0. \tag{10}$$

Here we have defined $V_C = \mathrm{Tr}(V_X)$ and $V_{C,\chi} = \frac{\partial V_C}{\partial\chi}\frac{16\pi G_5 N_f}{L^3 N_c} \to \lambda_0$.

For a two-flavor system in the graviton-dilaton-scalar framework, the deformed metric is self-consistently solved by considering both the chiral condensate and nonperturbative gluodynamics in the vacuum, which are responsible for the chiral symmetry breaking and linear confinement, respectively. The mixing between the chiral condensate and gluon condensate is important to produce the correct light-flavor meson spectra [46].

III. PHASE TRANSITION AND EQUATIONS OF STATE

The chiral and deconfinement phase transitions for the graviton-dilaton-scalar system will be investigated in the near future. In this section, we will focus on the deconfinement phase transition for the pure gluon system described by Eq. (1).

The finite temperature dynamics of gauge theories has a natural holographic counterpart in the thermodynamics of black holes on the gravity side. Adding the black-hole background to the holographic QCD model constructed from vacuum properties, in the string frame we have

$$ds_S^2 = e^{2A_s}\left(-f(z)dt^2 + \frac{dz^2}{f(z)} + dx^i dx^i\right). \tag{11}$$

The metric in the string frame is useful to calculate the jet quenching parameter.

The thermodynamical properties of the equation of state is convenient to be derived in the Einstein frame,

$$ds_E^2 = e^{2A_s - \frac{4\Phi}{3}}\left(-f(z)dt^2 + \frac{dz^2}{f(z)} + dx^i dx^i\right). \quad (12)$$

Under the frame transformation

$$g^E_{mn} = g^s_{mn} e^{-2\Phi/3}, \qquad V^E_G = e^{4\Phi/3} V^s_G, \quad (13)$$

Eq. (1) becomes

$$S^E_G = \frac{1}{16\pi G_5}\int d^5x\sqrt{g_E}\left(R_E - \frac{4}{3}\partial_m\Phi\partial^m\Phi - V^E_G(\Phi)\right). \quad (14)$$

We can derive the following equations from the Einstein equations of (t,t), (z,z), and (x_1,x_1) components:

$$-A_s'' + A_s'^2 + \frac{2}{3}\Phi'' - \frac{4}{3}A_s'\Phi' = 0, \quad (15)$$

$$f''(z) + (3A_s'(z) - 2\Phi'(z))f'(z) = 0. \quad (16)$$

The equation of motion of the dilaton field is given as the following:

$$\frac{8}{3}\partial_z(e^{3A_s(z)-2\Phi}f(z)\partial_z\Phi) - e^{5A_s(z)-\frac{10}{3}\Phi}\partial_\Phi V^E_G = 0. \quad (17)$$

To get the solutions, we impose the asymptotic AdS_5 condition $f(0) = 1$ near the UV boundary $z \sim 0$, and require Φ, f to be finite at $z = 0, z_h$ with z_h the black-hole horizon. Fortunately, we find that the solution of the black-hole background takes the form of

$$f(z) = 1 - f_c^h\int_0^z e^{-3A_s(z')+2\Phi(z')}dz', \quad (18)$$

with

$$f_c^h = \frac{1}{\int_0^{z_h} e^{-3A_s(z')+2\Phi(z')}dz'}. \quad (19)$$

A black-hole solution with a regular horizon is characterized by the existence of a surface $z = z_h$, where $f(z_h) = 0$. The Euclidean version of the solution is defined only for $0 < z < z_h$. In order to avoid the conical singularity, the periodicity of the Euclidean time can be fixed by

$$\tau \to \tau + \frac{4\pi}{|f'(z_h)|}. \quad (20)$$

This determines the temperature of the solution as

$$T = \frac{|f'(z_h)|}{4\pi}. \quad (21)$$

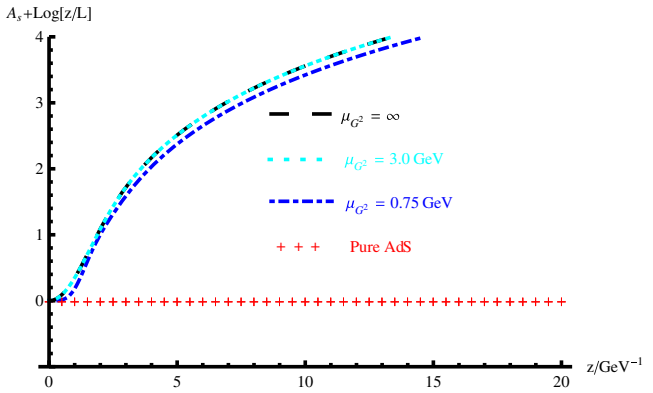

FIG. 2 (color online). A_s configurations compared with the AdS_5 metric for $G_5 = 1.25$ and $\mu_G = 0.75$ GeV and $\mu_{G^2} = \mu_G = 0.75$ GeV, $\mu_{G^2} = 3$ GeV, and $\mu_{G^2} = \infty$, respectively. To show the configuration smoothly, we have subtracted the $\log(z)$ divergence in A_s.

From Eq. (18), one can easily read out the relation between the temperature and position of the black-hole horizon,

$$T = \frac{e^{-3A_s(z_h)+2\Phi(z_h)}}{4\pi\int_0^{z_h} e^{-3A_s(z')+2\Phi(z')}dz'}. \quad (22)$$

For numerical calculations, we take $\mu_G = 0.75$ GeV in Eq. (3) so that the transition temperature is around 255 MeV, and we take three different values for μ_{G^2}: $\mu_{G^2} = \mu_G = 0.75$ GeV, $\mu_{G^2} = 3$ GeV, and $\mu_{G^2} = \infty$. When $\mu_{G^2} = \infty$, the dilaton field Eq. (3) takes the form of a quadratic term $\Phi = \mu_G^2 z^2$, and the model can be regarded as the self-consistent KKSS model. The only difference is that in this model, the metric structure is self-consistently deformed by the dilaton background, while in the KKSS model, the metric structure takes the same as AdS_5.

We can solve A_s from Eq. (15), and the results of the A_s configurations for $\mu_G = 0.75$ GeV and $\mu_{G^2} = 0.75$ GeV, $\mu_{G^2} = 3$ GeV, and $\mu_{G^2} = \infty$ are shown in Fig. 2. To show the configuration smoothly, we have subtracted the $\log(z)$ divergence in A_s. Comparing with the AdS_5 metric, it is easy to find that the metric structure is largely deformed at IR regime by the dilaton background field or gluodynamics. The two cases $\mu_{G^2} = 3$ GeV and $\mu_{G^2} = \infty$ are almost the same.

From Eqs. (16) and (22), we can get the $f(z)$ solution and the temperature behavior. The temperature vs horizon for $\mu_G = 0.75$ GeV and $\mu_{G^2} = 0.75$ GeV, $\mu_{G^2} = 3$ GeV, and $\mu_{G^2} = \infty$ are shown in Fig. 3. As long as μ_{G^2} is large, the IR physics is not sensitive to large μ_{G^2}, and the behaviors for $\mu_{G^2} = 3$ GeV and $\mu_{G^2} = \infty$ are almost the same. From Fig. 3, it is noticed that for a pure AdS_5-Schwarz black hole, the temperature monotonically decreases with the increasing of the horizon. If one solves the dual black-hole background self-consistently, one can find that there is a minimal temperature $T_{\min} = 255$ MeV at a certain black-hole horizon z_h^0. This is similar to the case

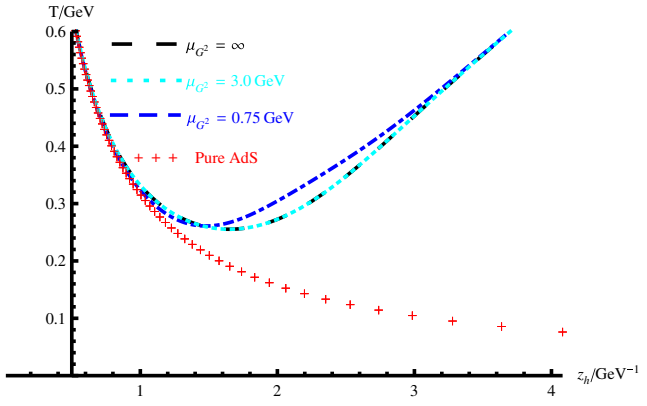

FIG. 3 (color online). The temperature as a function of horizon for $G_5 = 1.25$ and $\mu_G = 0.75$ GeV and $\mu_{G^2} = 0.75$ GeV, $\mu_{G^2} = 3$ GeV, and $\mu_{G^2} = \infty$, respectively. The blue lines stand for cases I and II, and the red lines are the results of the AdS-Schwarz black hole.

for the confining theory (at zero temperature) discussed in Ref. [37]. For $T < T_{\min}$, there are no black-hole solutions. For $T > T_{\min}$, there are two branches of black-hole solutions. When $z_h < z_h^0$, the temperature increases with the decreasing of z_h, which means that the temperature increases when the horizon moves close to UV regime, this phase is thermodynamically stable. When $z_h > z_h^0$, the temperature increases with the increase of z_h, which means that the temperature becomes higher and higher when the horizon moves to IR regime. This indicates that the solution for the branch $z_h > z_h^0$ is unstable and, thus, not physical. In order to determine the critical temperature, we have to compare the free energy difference between the stable black-hole solution and the thermal gas. Following the discussion in Ref. [39], the transition temperature would be near this minimal temperature, and we would just take it as the transition temperature $T_c = 255$ MeV, which is in agreement with the lattice result for the pure gluon system.

From the Bekenstein-Hawking formula, one can easily read the black-hole entropy density s, which is defined by the area A_{area} of the horizon:

$$s = \frac{A_{\text{area}}}{4G_5 V_3}\bigg|_{z_h} = \frac{1}{4G_5} e^{3A_s(z_h)-2\Phi(z_h)}, \tag{23}$$

where G_5 is the Newton constant in 5D curved space, and V_3 is the volume of the spatial directions. It is noticed that the entropy density is closely related to the metric in the Einstein frame. The results of the scaling entropy density s/T^3 for $\mu_G = 0.75$ GeV and $\mu_{G^2} = 0.75$ GeV, $\mu_{G^2} = 3$ GeV, and $\mu_{G^2} = \infty$ are shown in Fig. 4 compared with the lattice results for the pure gluon system [29]. It can be seen that when μ_{G^2} is large enough, the result is not sensitive to the value of μ_{G^2}, and it takes almost the same as that in the self-consistent KKSS model. The entropy density for $\mu_{G^2} = 3$ GeV to $\mu_{G^2} = \infty$ agrees well with the lattice result for pure $SU(3)$ gauge theory.

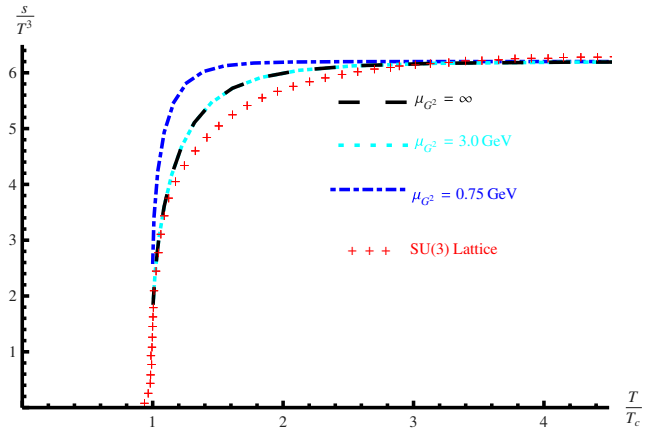

FIG. 4 (color online). The entropy density as a function of T/T_c for $G_5 = 1.25$ and $\mu_G = 0.75$ GeV and $\mu_{G^2} = 0.75$ GeV, $\mu_{G^2} = 3$ GeV, and $\mu_{G^2} = \infty$, respectively. The red crosses are lattice results from Ref. [29].

The pressure density $p(T)$ can be calculated from the entropy density $s(T)$ by solving the equation

$$\frac{dp(T)}{dT} = s(T), \tag{24}$$

and the energy density is related to the entropy density by

$$\varepsilon = -p + sT. \tag{25}$$

The trace anomaly $(\varepsilon - 3p)/T^4$ for $\mu_G = 0.75$ GeV and $\mu_{G^2} = 0.75$ GeV, $\mu_{G^2} = 3$ GeV, and $\mu_{G^2} = \infty$ are shown in Fig. 5 compared with lattice results for the pure gluon system [29]. The trace anomaly shows a peak around $T/T_c = 1.1$. When $\mu_{G^2} = 0.75$ GeV, the height of the peak is around 3.7, and when $\mu_{G^2} = 3$ GeV $\sim\infty$, the height reduces to 2.7, which agrees with the lattice data for pure

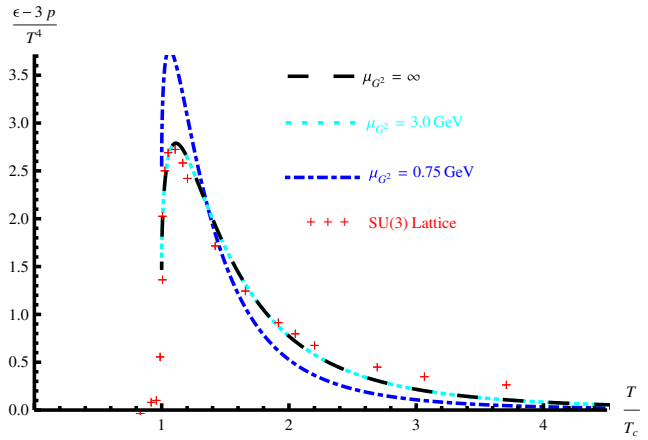

FIG. 5 (color online). Trace anomaly as a function of T/T_c for $G_5 = 1.25$ and $\mu_G = 0.75$ GeV and $\mu_{G^2} = 0.75$ GeV, $\mu_{G^2} = 3$ GeV, and $\mu_{G^2} = \infty$, respectively. The red crosses are lattice results from Ref. [29].

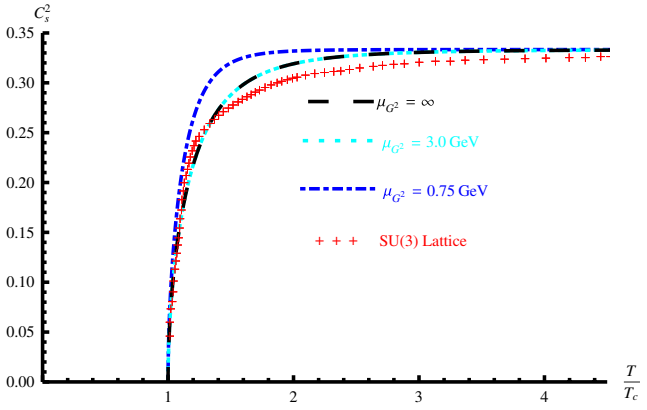

FIG. 6 (color online). The square of the sound velocity c_s^2 as a function of scaled temperature T/T_c for $G_5 = 1.25$ and $\mu_G = 0.75$ GeV and $\mu_{G^2} = 0.75$ GeV, $\mu_{G^2} = 3$ GeV and $\mu_{G^2} = \infty$, respectively. The red crosses are lattice results from Ref. [29].

$SU(3)$ gauge theory, as shown in Ref. [29]. At very high temperature, the trace anomaly goes to zero, which indicates the system is asymptotically conformal at high temperature.

The sound velocity c_s^2 can be obtained from the temperature and entropy:

$$c_s^2 = \frac{d\log T}{d\log s} = \frac{s}{T ds/dT}, \tag{26}$$

which can directly measure the conformality of the system. For the conformal system, $c_s^2 = 1/3$, for the nonconformal system, c_s^2 will deviate from $1/3$. From Eq. (26), we can see that the speed of the sound is independent of the normalization of the 5D Newton constant G_5 and the space volume V_3.

The numerical result of the square of the sound velocity is shown in Fig. 6. At T_c, the sound velocity square is around 0, which is in agreement with the lattice data [29]. At high temperature, the sound velocity square goes to $1/3$, which means that the system is asymptotically conformal.

IV. JET QUENCHING PARAMETER $\hat{Q}$

Jet quenching measures the strength of an energetic partons interacting with the created hot dense medium. It is very important to find the characterization of the resulting medium-induced modification of high-p_T parton fragmentation, i.e., jet quenching and its connection to properties of the hot dense matter, and whether and how such a parameter can tell us about the QCD phase transitions.

It has been expected that the shear-viscosity-over-entropy-density ratio η/s has a minimum in the QCD phase transition region [12] as that in systems of water, helium, and nitrogen [9,10]. The bulk viscosity ζ/s also exhibits a sharp rising behavior around the critical temperature T_c as shown in lattice QCD [23–25] and some model calculations [26,28]. It has been suggested in Ref. [13] that shear viscosity η/s and the jet quenching parameter $\hat{q}/T^3$ for a quasiparticle-dominated quark-gluon plasma have a general relation $\eta/s \sim T^3/\hat{q}$. If we naively extend this relation to the critical temperature region, we expect that $\hat{q}/T^3$ will show a peak around the critical temperature T_c. Phenomenologically, the strong NTcE scenario of jet-medium interaction [16] was proposed in the efforts to explain the large jet quenching anisotropy at high p_t at the RHIC [17–20].

There are no model calculations for the jet quenching parameter around the critical temperature. Lattice QCD is not suitable for transport properties. Recently, there have been several groups making efforts to calculate the jet quenching parameter on the lattice [49,50]. However, no information on the jet quenching parameter has been extracted around the critical temperature. In this section, we will investigate the jet quenching parameter around the critical temperature in the dynamical holographic QCD model which can describe phase transitions.

Following Ref. [35] (see, also, Refs. [51–53]), the jet quenching parameter is related to the adjoint Wilson loop by

$$W^{\mathrm{Adj}}[\mathcal{C}] \approx \exp\left(-\frac{1}{4\sqrt{2}}\hat{q}L^- L^2\right), \tag{27}$$

where L^-, L are distances along $x^- = \frac{t-x_1}{\sqrt{2}}$ and the spatial direction x_2, respectively. (Another method for jet quenching of light quarks has been developed in Ref. [54].)

Denoting $x^+ = \frac{t+x_1}{\sqrt{2}}, x^- = \frac{t-x_1}{\sqrt{2}}$, then the metric in Eq. (11) becomes

$$ds^2 = e^{2A_s}\left\{dx^- dx^+ + \frac{1-f(z)}{2}[dx^{+2} + dx^{-2}] + \frac{1}{f(z)}dz^2 + dx_2^2 + dx_3^2\right\}. \tag{28}$$

The action on the string world sheet is taken to be

$$S_{NG} = \frac{1}{2\pi\alpha'}\int d^2\sigma\sqrt{-\det(G_{\alpha\beta})}, \tag{29}$$

with $G_{\alpha\beta} = g^s_{\mu\nu}\partial_\alpha x^\mu \partial_\beta x^\nu$ the induced metric on the string world sheet.

With the above configuration in Fig. 7, we have

$$S_1 = \frac{1}{2\pi\alpha'}\int d\tau d\sigma\sqrt{g_{--}g_{zz}z'^2(\sigma) + g_{--}g_{22}}, \tag{30}$$

and with the below configuration in Fig. 7, we have

$$S_2 = \frac{1}{2\pi\alpha'}\int d\tau d\sigma\sqrt{g_{--}g_{zz}}, \tag{31}$$

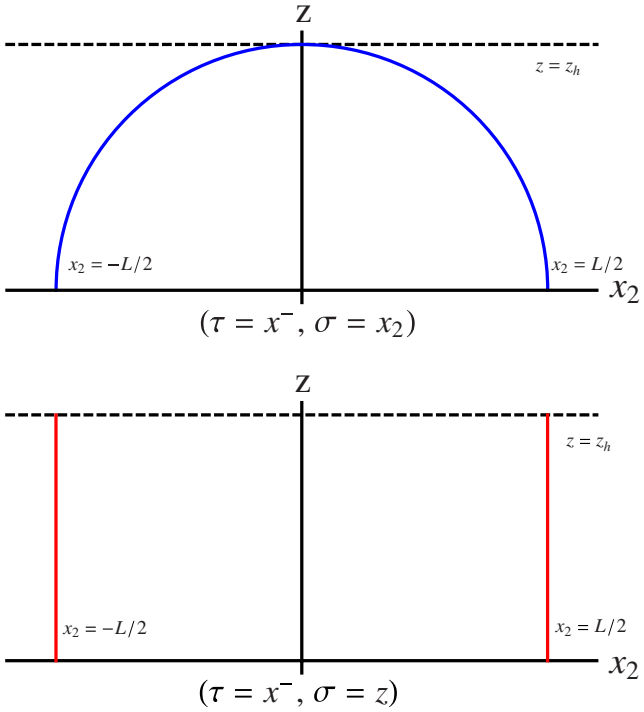

FIG. 7 (color online). Two kinds of string configurations.

where $g_{--} = e^{2A_s}\frac{1-f(z)}{2}$, $g_{zz} = \frac{e^{2A_s}}{f(z)}$, $g_{22} = e^{2A_s}$ can be read from Eq. (28).

Then we extract the adjoint Wilson loop by

$$W^{\mathrm{Adj}} = \exp(2i(S_1 - S_2)), \tag{32}$$

and from the small L expansion of W^{Adj}, we get $\hat{q}$ of the form

$$\hat{q} = \frac{\sqrt{2}\sqrt{\lambda}}{\pi \int_0^{z_h} dz \sqrt{g_{zz}/(g_{22}^2 g_{--})}}, \tag{33}$$

with $\sqrt{\lambda} = \frac{R^2_{\mathrm{AdS}}}{\alpha'}$.

In order to be more comprehensive, by transforming the integral variable from z to dimensionless variable $\nu = z/z_h$, we rewrite the above equation as

$$\hat{q} = \frac{\sqrt{2}\sqrt{\lambda}}{\pi z_h^3 \int_0^1 d\nu \sqrt{\frac{e^{-4A_s(\nu z_h)}}{z_h^4}\frac{1-f(\nu z_h)}{2} f(\nu z_h)}}. \tag{34}$$

In the AdS-Schwarz black-hole case, $f(z) = 1 - z^4/z_h^4 = 1 - \nu^4$, $1 - f(z) = \nu^4$, and $e^{-4A_s(z)}/z_h^4 = z^4/z_h^4 = \nu^4$ only depend on ν. Therefore, the integral kernel in the above equation would only depend on ν, and we have $\hat{q} \propto 1/z_h^3 \propto T^3$, which is the result of the conformal background. However, if we introduce a scale through the dilaton field in the form of Eq. (3) to break the conformality, from Eqs. (15) and (16), it is easy to see that in this case, $f(z)$ and $A_s(z)$ would depend on μ_G and μ_G^2. Correspondingly, from dimension analysis it is easy to see that after rescaling the integral variable, the integral kernel

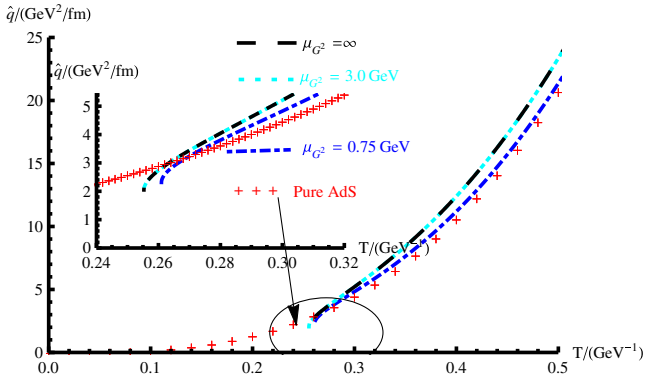

FIG. 8 (color online). Jet quenching parameter as a function of the temperature T for $\mu_G = 0.75$ GeV and $\mu_{G^2} = 0.75$ GeV, $\mu_{G^2} = 3$ GeV, and $\mu_{G^2} = \infty$ with $G_5 = 1.25$. The red crosses are the results of the AdS-SW black hole in Ref. [35]. We have taken $\lambda = 6\pi$ here.

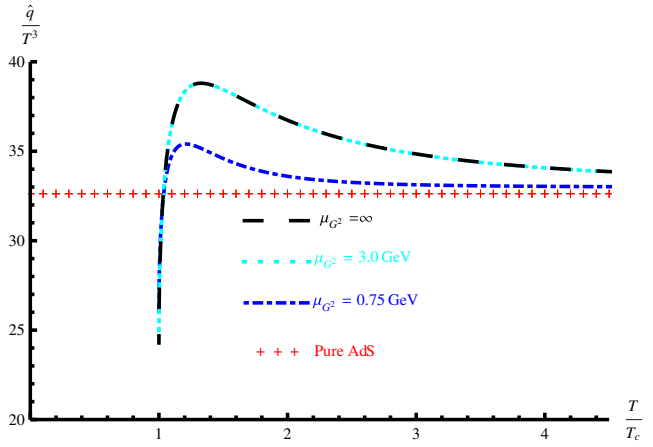

FIG. 9 (color online). Jet quenching parameter over cubic temperature $\hat{q}/T^3$ as a function of T/T_c for $\mu_G = 0.75$ GeV and $\mu_{G^2} = 0.75$ GeV, $\mu_{G^2} = 3$ GeV, and $\mu_{G^2} = \infty$ with $G_5 = 1.25$. The red crosses are the results of the AdS-SW black hole in Ref. [35]. We have taken $\lambda = 6\pi$ here.

in Eq. (34) would depend not only on ν but also on $\mu_G z_h$ and $\mu_{G^2} z_h$, and the integral part would have extra contribution dependent on z_h. As a result, we expect the result of $\hat{q}/T^3$ would no longer be a constant but depend on T through the dependence on z_h.

The numerical results of the jet quenching parameter $\hat{q}$ and the ratio of $\hat{q}/T^3$ for $\mu_G = 0.75$ GeV and $\mu_{G^2} = 0.75$ GeV, $\mu_{G^2} = 3$ GeV, and $\mu_{G^2} = \infty$ are shown in Figs. 8 and 9, respectively. The results are compared with the AdS_5 case. For all the cases, we have taken $\lambda = 6\pi$ as in Ref. [35]. It is found that the jet quenching parameter $\hat{q}$ itself does not show much difference for all the cases. It is even hard to find much difference comparing with the AdS_5 case. For all these cases, the value of $\hat{q}$ is around $5 - 10$ GeV^2/fm in the temperature range 300–400 MeV, which is in agreement with the lattice result in Ref. [50]. However, the ratio $\hat{q}/T^3$ shows very different behavior for different cases: For the AdS_5 case,

the ratio is a constant; for the dynamical holographic QCD model, which can describe the deconfinement phase transition, we can find that $\hat{q}/T^3$, indeed, shows a peak at the same temperature where the trace anomaly also shows a peak. For the case of $\mu_{G^2} = 3$ GeV $\sim \infty$, the height of the peak is around 40 at $T = 1.1T_c$.

It is worth mentioning that our $\hat{q}$ is very dependent on the value of the 't Hooft coupling λ, which, at the moment, is a free parameter. In the recent work [55], the jet quenching parameter $\hat{q}$ extracted from experiment is around 1.1 GeV^2/fm at $T = 370$MeV and 1.9 GeV^2/fm for $T = 470$ MeV, which is 5 times smaller than our results. This might indicate that we should take a smaller 't Hooft coupling. However, the temperature-dependent feature is independent of the 't Hooft coupling.

V. JET QUENCHING CHARACTERIZING THE PHASE TRANSITION

We have observed that both the $\hat{q}/T^3$ and trace anomaly $(\varepsilon - 3p)/T^4$ show a peak around the critical temperature for $\mu_G = 0.75$ GeV, which indicates that the jet quenching parameter over the cubic temperature can characterize the QCD phase transition. In this section, we explore how different values of μ_G affect the phase transition and jet quenching. From Refs. [45,46], μ_G is related to the linear confinement and determines the Regge slope of the glueball spectra as well as the string tension of the linear quark potential.

In Figs. 10 and 11, we show the behavior of the $\hat{q}/T^3$ and trace anomaly $(\varepsilon - 3p)/T^4$ for different values of μ_G as a function of temperature T and scaled T/T_c, respectively.

From Fig. 10, we find that for different values of μ_G (with $\mu_{G^2} \to \infty$), the critical temperature T_c increases with μ_G. We can read $T_c = 146, 170, 204, 255$ MeV for $\mu_G = 0.43, 0.5, 0.6, 0.7$ GeV, respectively. It is also observed that the height of the peak for either $\hat{q}/T^3$ or $(\varepsilon - 3p)/T^4$ does not change with the value of μ_G, but the width of the peak increases with μ_G.

Another interesting observation from Fig. 11 is that neither $\hat{q}/T^3$ nor $(\varepsilon - 3p)/T^4$ as a function of scaled T/T_c is sensitive to μ_G, i.e., $\hat{q}/T^3(T/T_c)$ or $(\varepsilon - 3p)/T^4(T/T_c)$ overlaps for different values of μ_G.

In the next section, we will investigate the nuclear modification R_{AA} and elliptic flow v_2, where the behavior

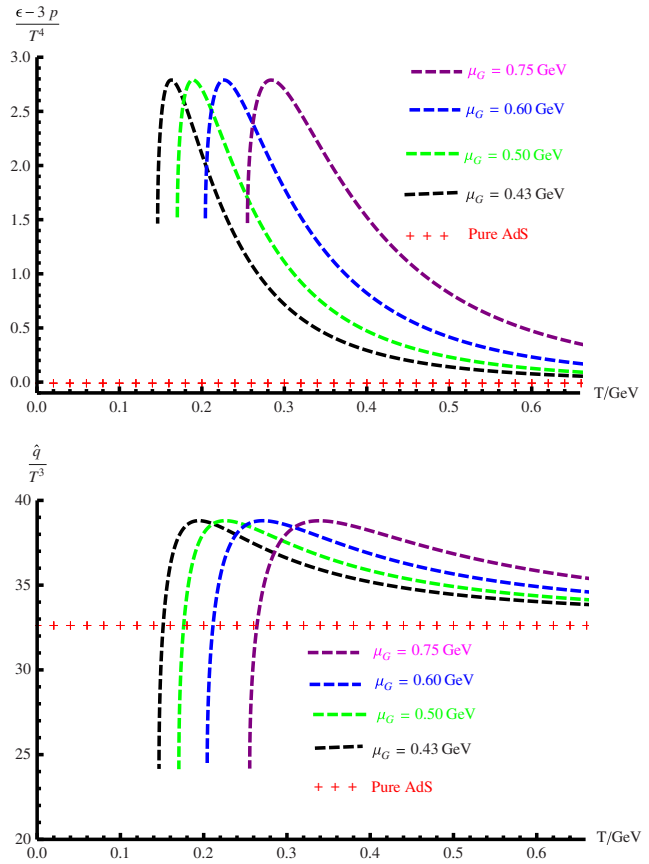

FIG. 10 (color online). $\hat{q}/T^3$ and trace anomaly $(\varepsilon - 3p)/T^4$ as a function of T for different values of μ_G with $\mu_{G^2} = 3$ GeV $\sim \infty$. The red crosses are for the AdS$_5$ case. We have taken $G_5 = 1.25$ and $\lambda = 6\pi$ here.

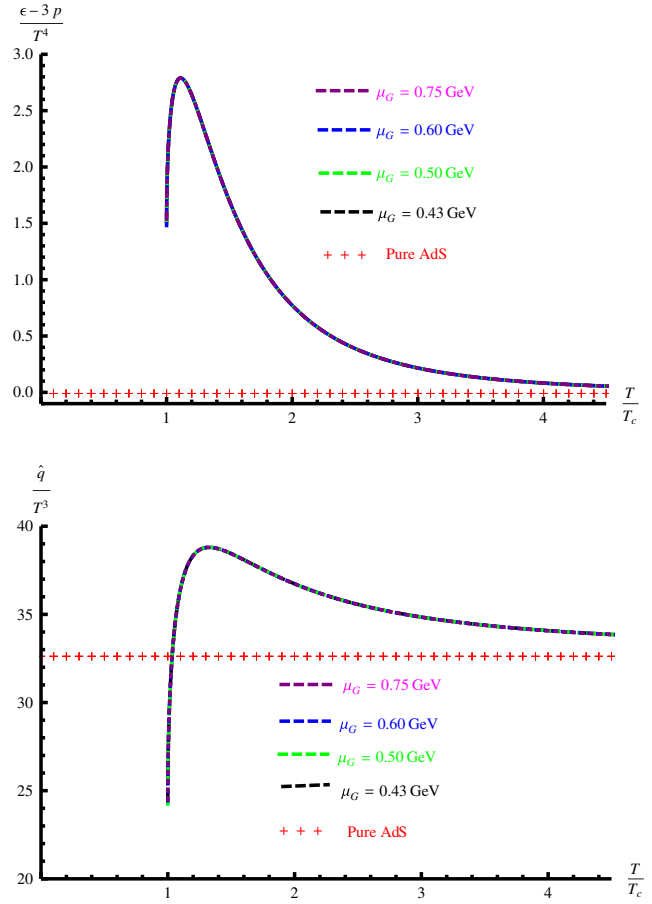

FIG. 11 (color online). $\hat{q}/T^3$ and trace anomaly $(\varepsilon - 3p)/T^4$ as a function of T/T_c for different values of μ_G with $\mu_{G^2} = 3$ GeV $\sim \infty$. The red crosses are for the AdS$_5$ case. We have taken $G_5 = 1.25$ and $\lambda = 6\pi$ here.

of $\hat{q}/s$ is needed. For the case of AdS_5, the temperature is $T = \frac{1}{\pi z_h}$, and the entropy density takes the form of

$$s_{AdS_5} = \frac{1}{4G_5}\frac{1}{z_h^3} = \frac{\pi^3}{4G_5}T^3 \simeq 7.75\frac{1}{G_5}T^3, \quad (35)$$

and the jet quenching parameter is given by

$$\hat{q}_{AdS_5} = \frac{\pi^{3/2}\sqrt{\lambda}\Gamma[3/4]}{\Gamma[5/4]}T^3 \simeq 7.53\sqrt{\lambda}T^3. \quad (36)$$

Therefore, in the AdS_5 limit, the ratio of the jet quenching parameter over the entropy density takes the value of

$$\hat{q}_{AdS_5}/s_{AdS_5} = 0.97G_5\sqrt{\lambda}. \quad (37)$$

With the parameters used in our work, we have $\hat{q}_{AdS_5}/s_{AdS_5} = 5.27$. The ratio of $\hat{q}/s$ in the dynamical holographic QCD model as a function of T and T/T_c is shown in Fig. 12 compared with the AdS_5 result. It is found that the ratio of $\hat{q}/s$ reaches the AdS_5 limit 5.27 at high temperature, and it sharply rises with the decreasing of T and develops a peak exactly at T_c with the height 16.3, which is about 3 times larger than its value at high temperature. It is worth mentioning that the sharp rising of $\hat{q}/s$ around T_c is very similar to the behavior of the bulk viscosity over entropy density ζ/s, as shown in Refs. [23,24].

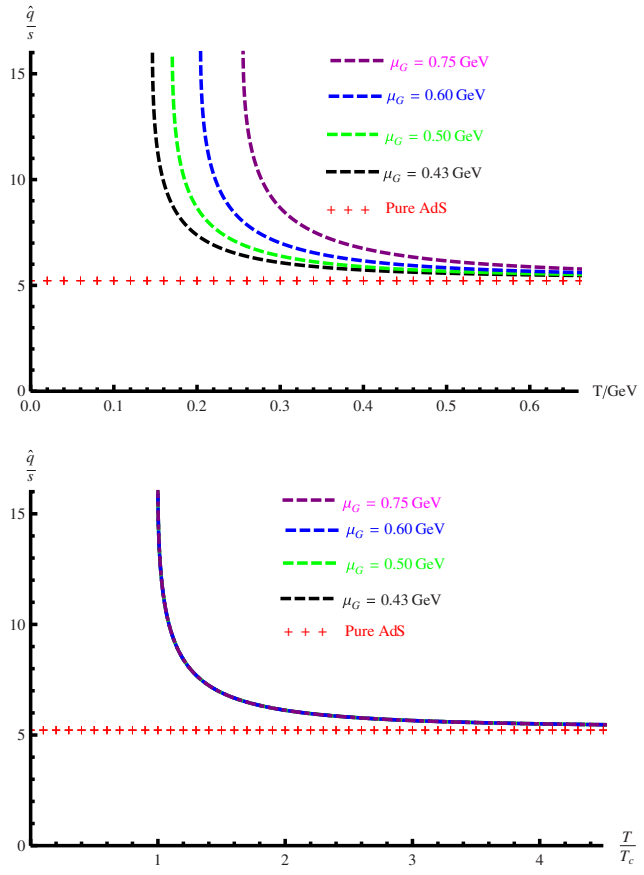

FIG. 12 (color online). $\hat{q}/s$ as a function of T and T/T_c for different values of μ_G with $\mu_{G^2} = 3$ GeV $\sim\infty$, respectively. The red crosses are for the AdS_5 case. We have taken $G_5 = 1.25$ and $\lambda = 6\pi$ here.

Moreover, $\hat{q}/s$ as a function of the scaled temperature T/T_c overlaps for different values of μ_G.

VI. JET QUENCHING PHENOMENOLOGY FROM HOLOGRAPHY

In this section, we study the phenomenological implications of the temperature dependence for $\hat{q}(T)$ as obtained from the holography model above. The observable commonly used for jet quenching phenomenology in AA collisions is the nuclear modification factor R_{AA} defined as the ratio between the hadron production in AA collision and that in NN collision (further scaled by the expected binary collision number). If a jet parton loses energy along its path penetrating the hot medium, one expects a significant suppression of leading high-p_t (transverse momentum) hadron production from the jet as compared with the pp collision at the same beam energy. A strong suppression was first observed at the RHIC [5] and then at the LHC [56], with R_{AA} reaching ~0.2 in the most central collisions. Another important aspect of jet quenching is the so-called geometric tomography [57] by measuring the azimuthal angle dependence of the suppression $R_{AA}(\phi)$, where ϕ is the angle of the produced hadron with respect to the reaction plane. In a typical off-central collision, the hot medium, on average, has an almondlike geometric shape, and, thus, the jet in-medium path length would depend on its orientation with respect to the matter geometry, leading to nontrivial dependence of the suppression on the azimuthal angle. The dominant component of the ϕ dependence is the second harmonic with its coefficient commonly referred to as v_2. Both the RHIC and LHC measurements have shown a sizable v_2 in the high-p_t region where the jet energy loss should be the mechanism of generating such anisotropy [58–61].

The key issue we focus on here is the temperature dependence of the jet-medium coupling, in particular, its possible nontrivial behavior near the parton/hadron phase boundary. As was first found in Ref. [16], the geometric anisotropy v_2 at high p_t is particularly sensitive to such temperature dependence, and a simultaneous description of high-p_T R_{AA} and v_2 at the RHIC requires a strong enhancement of jet-medium coupling in the near-T_c region. The near-T_c enhancement of jet-medium interaction as a generic mechanism has been further studied in many later works and shown to increase the jet azimuthal anisotropy with fixed overall suppression. Furthermore, how the overall opaqueness of the created fireball evolves with collisional beam energy is also very sensitive to such temperature dependence. From the RHIC to LHC, the

collision beam energy increases by a little more than 10 times, and the matter density increases (in most central collisions) by a factor of about 2. Such a span from the RHIC to LHC provides an opportunity for determining how the jet-medium interaction changes with the temperature. In particular, the near-T_c enhancement predicts a visible reduction of average opaqueness of the fireball from the RHIC to LHC. A number of recent analyses have consistently reported that the R_{AA} data at the RHIC and LHC, indeed, suggest an ~30% reduction of jet-medium interaction at the LHC as compared to the RHIC [21,22,62–67]. Therefore, phenomenologically, it appears that there is now strong evidence for a nontrivial temperature dependence, in particular, the near-T_c enhancement of jet-medium coupling on matter temperature.

Theoretically, however, there has been a very limited way to figure out the precise form of such T dependence due to the highly nonperturbative nature of this temperature regime. The holographic approach provides a useful way to gain insight into this problem. In the previous section, we used the holographic QCD model with nonconformal dynamics to calculate the $\hat{q}(T)$. As clearly seen in Fig. 9, the scaled jet-medium coupling $\hat{q}/T^3$ shows strong enhancement in the vicinity of T_c, while, in contrast, any conformal holographic model will show no T dependence for the $\hat{q}/T^3$. We also emphasize that the same holographic model describes the trace anomaly (with a strong peak near T_c) in thermodynamics. With such T dependence obtained from the holographic model here, it is of great interest to see its phenomenological implications. Here we use the simple geometric energy loss model as in Refs. [16,62] to study the R_{AA} and v_2 at high p_t for the RHIC, which are most sensitive to such T dependence. Let us assume that the final energy E_f of a jet with initial energy E_i after traveling an in-medium path $\vec{P}$ (specified by the jet initial spot and momentum direction) can be parametrized as $E_f = E_i \times f_{\vec{P}}$ with the $f_{\vec{P}}$ given by

$$f_{\vec{P}} = \exp\left\{-\int_{\vec{P}} \kappa[s(l)]s(l)ldl\right\}. \tag{38}$$

Here, $s(l)$ is the local entropy density along the jet path, while the $\kappa(s)$ represents the local jet-medium interaction strength which depends on the local density $s(l)$ (or, equivalently, the temperature T). We choose to explicitly separate out the density s itself, and the combination $\kappa(s)s$ corresponds to $\hat{q}$. To implement the holographic model results for $\hat{q}$, we use $\kappa[s] = \xi[\hat{q}/T^3]$ with $\hat{q}/T^3$ given as in Fig. 9 and with ξ just one parameter to be fixed by the most central collisions $R_{AA} \approx 0.18$ for 0%–5% centrality class and then used for other computations. We use optical the Glauber model to sample initial jet spots according to binary collision density, and we determine a medium density from a participant density with longitudinal boost-invariant expansion. There are strong initial state fluctuations, which could also contribute. But since we are focusing on the average R_{AA} and the dominant geometric anisotropy component v_2 is from geometry dominantly, the current approach is reasonable (for detailed discussions of the initial fluctuations for the hard probe, see, e.g., Refs. [21,22,68]). In our simulations for each given impact parameter, we compute the energy loss for 1×10^6 jet paths with different initial spots and orientations and extract the R_{AA}:

$$R_{AA}(\phi) = \langle (f_{\vec{P}_\phi})^{n-2} \rangle_{\vec{P}_\phi}, \tag{39}$$

where $\langle\rangle_{\vec{P}_\phi}$ means averaging over all jet paths with azimuthal orientation ϕ and including all sampled initial jet production spots. The exponent n comes from the reference pp spectrum at the same collision energy: $n \approx 8.1$ and 6.0 for $\sqrt{s} = 0.2$ and 2.76 TeV. The so-obtained $R_{AA}(\phi)$ in each event can be further Fourier decomposed as $R_{AA}(\phi) = R_{AA}[1 + 2v_2 \cos(2\phi)]$. The overall quenching R_{AA} as well as the azimuthal anisotropy v_2 can then be determined. While the jet energy loss anisotropy we discuss here arises from the geometric origin with the plasma being locally isotropic, it should be pointed out that additional angular dependence of energy loss might also occur due to intrinsic anisotropy within the local plasma; see, e.g., studies of jet quenching in strongly coupled anisotropic plasma in Refs. [69,70].

In Fig. 13, we show the results for R_{AA} and v_2 at high p_t for the RHIC with the input T-dependent jet-medium interaction from our nonconformal holographic model (the thick blue curves). For comparison, we also show the results from the conformal model, i.e., with $\hat{q}/T^3$ being constant in the QGP phase (the thin red curves). The data are from PHENIX measurements in Ref. [58]. As one can see, while both types of models describe the R_{AA} well, the nonconformal model shows a sizable improvement over the conformal model in getting closer to the data. Of course, our current nonconformal model still does not give enough anisotropy, which implies that the T dependence of the jet-medium coupling in this model may still show less near-T_c enhancement than the phenomenologically favored form. Such discrepancy at a quantitative level may not be unexpected due to a number of issues. After all, the holographic model used here is supposed to be an effective description dual to pure gluodynamics and, strictly speaking, may not be suitable for direct application to full QCD phenomenology. First of all, in a real QCD case with crossover transition, there is the "hadronic" side (i.e., the sizable contribution for $\hat{q}$ when T is smaller but close to T_c) [71], which is missing in the current holographic model with first order transition. Furthermore, the entropy density here (only counting the gluons, essentially) is also different from full QCD where there are quarks too, and that, in general, would shift the peak toward the lower

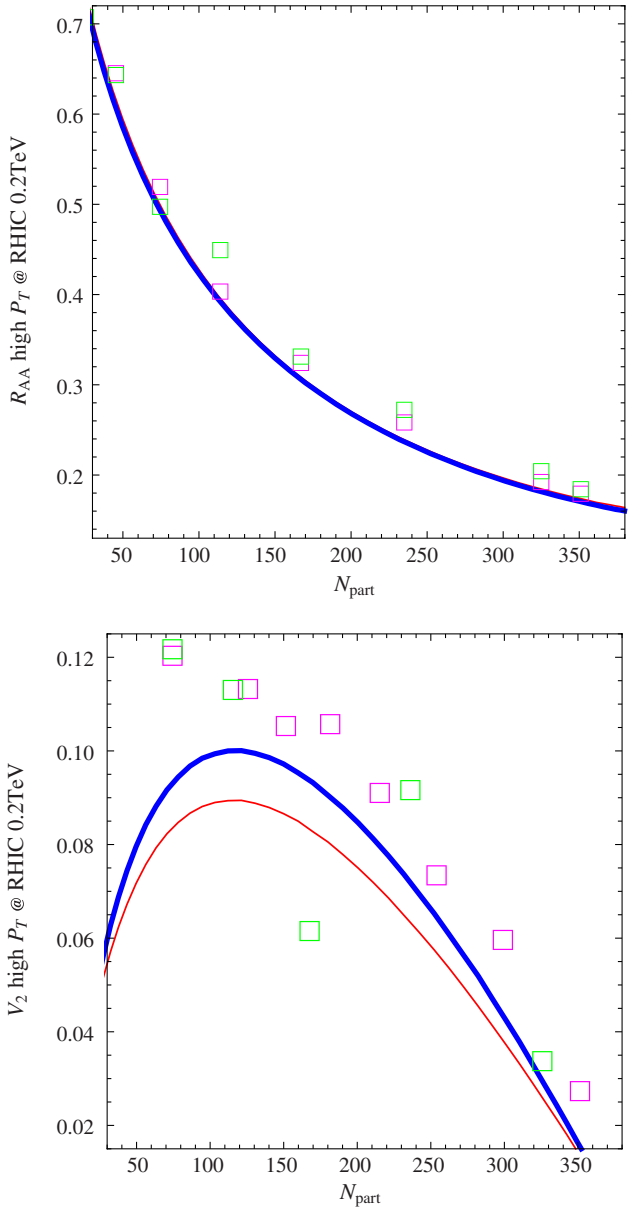

FIG. 13 (color online). The R_{AA} (upper) and v_2 (lower) at high p_t as a function of participant number $N_{\rm part}$ for the RHIC. The thick blue curves are the results from the nonconformal holographic model with $\hat{q}/T^3$ given in Fig. 9 ($\mu_G = 0.75$ GeV, $T_c = 255$ MeV), while the thin red curves are from the conformal model with $\hat{q}/T^3$ being constant. The data are PHENIX measurements of neutral pions for the kinematic range of $6 < p_t < 9$ GeV and $p_t > 9$ GeV.

density region in the present model. One might attempt to "cook up" certain extrapolative ways of accounting for such differences and, thus, improve the agreement with the data. We, however, feel that would weaken the internal rigor and consistency of the holographic model approach and would add very little to our main purpose, which is not to claim success in the description of the data but to demonstrate the consequence of nonconformal dynamics in our holographic model on the jet energy loss phenomenology.

Let us end by reiterating our main points here: (1) There are strong nonconformal, nonperturbative dynamics going on in the near-T_c region (which is modeled via holography here by introducing quadratic terms); (2) such dynamics leads to nonmonotonic behavior in QGP thermodynamics as shown by the strong near-T_c peak of the trace anomaly (which is well modeled by holography); (3) the same dynamics leads to nonmonotonic behavior in the QGP transport properties and, in particular, strong near-T_c enhancement of the jet-medium coupling; (4) phenomenologically, the T dependence of $\hat{q}$ from the nonconformal holographic model considerably improves the description of jet quenching azimuthal anisotropy as compared with the conformal case.

VII. SUMMARY

We have investigated QCD phase transition and jet quenching parameter $\hat{q}$ in the framework of a dynamical holographic QCD model. The thermodynamical properties in this dynamical holographic QCD model agree well with lattice results for a pure gluon system. It was found that both the trace anomaly $(\varepsilon - 3p)/T^4$ and the ratio of the jet quenching parameter over cubic temperature $\hat{q}/T^3$ show a peak around the critical temperature T_c. It was also noticed that the ratio of jet quenching parameter over entropy density $\hat{q}/s$ sharply rises at T_c, which is similar to the behavior of bulk viscosity over entropy density ζ/s. The enhancement of the jet quenching parameter around T_c indicated that, like the ratio of shear viscosity over entropy density η/s and the ratio of bulk viscosity over entropy density ζ/s, the ratio of jet quenching parameter over entropy density $\hat{q}/s$ can also characterize the phase transition.

The effect of jet quenching parameter enhancement around the phase transition on nuclear modification factor R_{AA} and elliptic flow v_2 were also been analyzed, and it was found that the T dependence of $\hat{q}$ from the nonconformal dynamical holographic model could considerably improve the description of jet quenching azimuthal anisotropy as compared with the conformal case.

Here are several remarks about the dynamical holographic QCD model we used in this work: (1) We have only considered the graviton-dilaton coupled system for the pure gluon system; it would be interesting to see in the future how the behavior of the jet quenching parameter changes by including dynamical quarks and how it will affect R_{AA} and v_2. (2) We have only considered the gluonic matter above T_c; one needs to construct the thermal gas below T_c in order to get the $\hat{q}/T^3$ behavior in the hadron gas. (3) One should also consider how to distinguish the energy loss of gluons and quarks [72] in the framework of holography QCD.

ACKNOWLEDGMENTS

This work is supported by the NSFC under Grant No. 11275213, DFG and NSFC (CRC 110), CAS key Project No. KJCX2-EW-N01, K. C. Wong Education Foundation, and the Youth Innovation Promotion Association of CAS. The research of J. L. is supported by the National Science Foundation under Grant No. PHY-1352368. J. L. is grateful to the RIKEN BNL Research Center for partial support.

[1] I. Arsene *et al.* (BRAHMS Collaboration), Nucl. Phys. **A757**, 1 (2005); K. Adcox *et al.* (PHENIX Collaboration), Nucl. Phys. **A757**, 184 (2005); B. B. Back *et al.*, Nucl. Phys. **A757**, 28 (2005); J. Adams *et al.* (STAR Collaboration), Nucl. Phys. **A757**, 102 (2005).
[2] M. Gyulassy and L. McLerran, Nucl. Phys. **A750**, 30 (2005).
[3] D. Teaney, J. Lauret, and E. V. Shuryak, Phys. Rev. Lett. **86**, 4783 (2001); P. Huovinen, P. F. Kolb, U. W. Heinz, P. V. Ruuskanen, and S. A. Voloshin, Phys. Lett. B **503**, 58 (2001); T. Hirano, U. W. Heinz, D. Kharzeev, R. Lacey, and Y. Nara, Phys. Lett. B **636**, 299 (2006); P. Romatschke and U. Romatschke, Phys. Rev. Lett. **99**, 172301 (2007); H. Song and U. W. Heinz, Phys. Lett. B **658**, 279 (2008); H. Song and U. W. Heinz, Phys. Rev. C **77**, 064901 (2008).
[4] A. Nakamura and S. Sakai, Phys. Rev. Lett. **94**, 072305 (2005).
[5] K. Adcox *et al.*, Phys. Rev. Lett. **88**, 022301 (2001); C. Adler *et al.*, Phys. Rev. Lett. **89**, 202301 (2002).
[6] R. Baier, Y. L. Dokshitzer, A. H. Mueller, S. Peigne, and D. Schiff, Nucl. Phys. **B483**, 291 (1997).
[7] M. Gyulassy and X.-N. Wang, Nucl. Phys. **B420**, 583 (1994); B. G. Zhakharov, JETP Lett. **63**, 952 (1996); U. Wiedemann, Nucl. Phys. **B588**, 303 (2000); M. Gyulassy, P. Lévai, and I. Vitev, Nucl. Phys. **B594**, 371 (2001).
[8] X. F. Guo and X.-N. Wang, Phys. Rev. Lett. **85**, 3591 (2000); X.-N. Wang and X. F. Guo, Nucl. Phys. **A696**, 788 (2001).
[9] L. P. Csernai, J. I. Kapusta, and L. D. McLerran, Phys. Rev. Lett. **97**, 152303 (2006).
[10] J. Liao and V. Koch, Phys. Rev. C **81**, 014902 (2010).
[11] Y. Hidaka and R. D. Pisarski, Phys. Rev. D **81**, 076002 (2010).
[12] J.-W. Chen, M. Huang, Y.-H. Li, E. Nakano, and D.-L. Yang, Phys. Lett. B **670**, 18 (2008).
[13] A. Majumder, B. Muller and X.-N. Wang, Phys. Rev. Lett. **99**, 192301 (2007).
[14] A. Rebhan and D. Steineder, Phys. Rev. Lett. **108**, 021601 (2012).
[15] D. Giataganas and H. Soltanpanahi, Phys. Rev. D **89**, 026011 (2014).
[16] J. Liao and E. Shuryak, Phys. Rev. Lett. **102**, 202302 (2009).
[17] J. Adams *et al.* (STAR Collaboration), Phys. Rev. C **72**, 014904 (2005).
[18] A. Adare *et al.* (PHENIX Collaboration), Phys. Rev. Lett. **105**, 142301 (2010).
[19] J. Jia and R. Wei, Phys. Rev. C **82**, 024902 (2010).
[20] J. Jia, W. A. Horowitz, and J. Liao, Phys. Rev. C **84**, 034904 (2011).
[21] X. Zhang and J. Liao, Phys. Rev. C **89**, 014907 (2014).
[22] X. Zhang and J. Liao, Phys. Rev. C **87**, 044910 (2013); Phys. Lett. B **713**, 35 (2012).
[23] D. Kharzeev and K. Tuchin, J. High Energy Phys. 09 (2008) 093; F. Karsch, D. Kharzeev, and K. Tuchin, Phys. Lett. B **663**, 217 (2008).
[24] H. B. Meyer, Phys. Rev. Lett. **100**, 162001 (2008).
[25] K. Huebner, F. Karsch, and C. Pica, Phys. Rev. D **78**, 094501 (2008).
[26] K. Paech and S. Pratt, Phys. Rev. C **74**, 014901 (2006).
[27] H. Mao, J. Jin, and M. Huang, J. Phys. G **37**, 035001 (2010).
[28] B. C. Li and M. Huang, Phys. Rev. D **78**, 117503 (2008).
[29] G. Boyd, J. Engels, F. Karsch, E. Laermann, C. Legeland, M. Lutgemeier, and B. Petersson, Nucl. Phys. **B469**, 419 (1996).
[30] M. Cheng *et al.*, Phys. Rev. D **77**, 014511 (2008).
[31] J. M. Maldacena, Adv. Theor. Math. Phys. **2**, 231 (1998).
[32] S. S. Gubser, I. R. Klebanov, and A. M. Polyakov, Phys. Lett. B **428**, 105 (1998).
[33] E. Witten, Adv. Theor. Math. Phys. **2**, 253 (1998).
[34] G. Policastro, D. T. Son, and A. O. Starinets, Phys. Rev. Lett. **87**, 081601 (2001); P. Kovtun, D. T. Son, and A. O. Starinets, Phys. Rev. Lett. **94**, 111601 (2005).
[35] H. Liu, K. Rajagopal, and U. A. Wiedemann, Phys. Rev. Lett. **97**, 182301 (2006).
[36] S. S. Gubser and A. Nellore, Phys. Rev. D **78**, 086007 (2008); S. S. Gubser, A. Nellore, S. S. Pufu, and F. D. Rocha, Phys. Rev. Lett. **101**, 131601 (2008); S. S. Gubser, S. S. Pufu, and F. D. Rocha, J. High Energy Phys. 08 (2008) 085.
[37] U. Gursoy, E. Kiritsis, L. Mazzanti, and F. Nitti, J. High Energy Phys. 05 (2009) 033; U. Gursoy, E. Kiritsis, L. Mazzanti, and F. Nitti, Phys. Rev. Lett. **101**, 181601 (2008); U. Gursoy, E. Kiritsis, G. Michalogiorgakis, and F. Nitti, J. High Energy Phys. 12 (2009) 056.
[38] E. Megias, H. J. Pirner, and K. Veschgini, Phys. Rev. D **83**, 056003 (2011); K. Veschgini, E. Megias, and H. J. Pirner, Phys. Lett. B **696**, 495 (2011).
[39] D. Li, S. He, M. Huang, and Q.-S. Yan, J. High Energy Phys. 09 (2011) 041.
[40] J. Erlich, E. Katz, D. T. Son, and M. A. Stephanov, Phys. Rev. Lett. **95**, 261602 (2005).
[41] A. Karch, E. Katz, D. T. Son, and M. A. Stephanov, Phys. Rev. D **74**, 015005 (2006).
[42] C. Csaki and M. Reece, J. High Energy Phys. 05 (2007) 062.
[43] T. Gherghetta, J. I. Kapusta, and T. M. Kelley, Phys. Rev. D **79**, 076003 (2009).

[44] Y.-Q. Sui, Y.-L. Wu, Z.-F. Xie, and Y.-B. Yang, Phys. Rev. D **81**, 014024 (2010); Y.-Q. Sui, Y.-L. Wu, and Y.-B. Yang, Phys. Rev. D **83**, 065030 (2011).
[45] D. Li, M. Huang, and Q.-S. Yan, Eur. Phys. J. C **73**, 2615 (2013).
[46] D. Li and M. Huang, J. High Energy Phys. 11 (2013) 088.
[47] D. Li and M. Huang, arXiv:1311.0593.
[48] A. Adams, L. D. Carr, T. Schaefer, P. Steinberg, and J. E. Thomas, New J. Phys. **14**, 115009 (2012).
[49] A. Majumder, Phys. Rev. C **87**, 034905 (2013).
[50] M. Panero, K. Rummukainen, and A. Schfer, Phys. Rev. Lett. **112**, 162001 (2014).
[51] U. Gursoy, E. Kiritsis, G. Michalogiorgakis, and F. Nitti, J. High Energy Phys. 12 (2009) 056.
[52] R.-G. Cai, S. Chakrabortty, S. He, and L. Li, J. High Energy Phys. 02 (2013) 068.
[53] Z.-q. Zhang, D.-f. Hou, and H.-c. Ren, J. High Energy Phys. 01 (2013) 032.
[54] A. Ficnar, S. S. Gubser, and M. Gyulassy, arXiv:1311.6160.
[55] K. M. Burke, A. Buzzatti, N. Chang, C. Gale, M. Gyulassy, U. Heinz, S. Jeon, A. Majumder *et al.*, arXiv:1312.5003.
[56] K. Aamodt *et al.* (ALICE Collaboration), Phys. Lett. B **696**, 30 (2011); S. Chatrchyan *et al.* (CMS Collaboration), Eur. Phys. J. C **72**, 1945 (2012).
[57] M. Gyulassy, I. Vitev, and X. N. Wang, Phys. Rev. Lett. **86**, 2537 (2001).
[58] A. Adare *et al.* (PHENIX Collaboration), Phys. Rev. Lett. **105**, 142301 (2010).
[59] B. Abelev *et al.* (ALICE Collaboration), Phys. Lett. B **719**, 18 (2013).
[60] G. Aad *et al.* (ATLAS Collaboration), Phys. Rev. C **86**, 014907 (2012); Phys. Lett. B **707**, 330 (2012).
[61] S. Chatrchyan *et al.* (CMS Collaboration), Phys. Rev. Lett. **109**, 022301 (2012).
[62] J. Liao, AIP Conf. Proc. **1441**, 874 (2012).
[63] W. A. Horowitz and M. Gyulassy, Nucl. Phys. **A872**, 265 (2011).
[64] B. Betz and M. Gyulassy, arXiv:1305.6458; Phys. Rev. C **86**, 024903 (2012).
[65] A. Buzzatti and M. Gyulassy, Nucl. Phys. **A904–A905**, 779c (2013).
[66] R. A. Lacey, N. N. Ajitanand, J. M. Alexander, J. Jia, and A. Taranenko, arXiv:1203.3605; arXiv:1202.5537.
[67] B. G. Zakharov, JETP Lett. **93**, 683 (2011); arXiv: 1105.0191.
[68] T. Renk, Phys. Rev. C **85**, 044903 (2012); T. Renk, H. Holopainen, J. Auvinen, and K. J. Eskola, Phys. Rev. C **85**, 044915 (2012); T. Renk, H. Holopainen, U. Heinz, and C. Shen, Phys. Rev. C **83**, 014910 (2011).
[69] D. Giataganas, J. High Energy Phys. 07 (2012) 031.
[70] M. Chernicoff, D. Fernandez, D. Mateos, and D. Trancanelli, J. High Energy Phys. 08 (2012) 041.
[71] C. Hidalgo-Duque and F. J. Llanes-Estrada, arXiv: 1309.7211.
[72] S. Lin, R. D. Pisarski, and V. V. Skokov, Phys. Lett. B **730**, 236 (2014).